Research Article | Vol. 29, No. 11 / 24 May 2021 / Optics Express 16904
Optics EXPRESS

Femtosecond laser patterned superhydrophobic/hydrophobic SERS sensors for rapid positioning ultratrace detection

HUAN YANG,[1] XIANGYUN GUN,[1] GIHONG PANG,[2,5] ZHIXIA ZHENG,[3] CHUNBO LI,[1] CAN YANG,[1] MENG WANG,[1] AND KAICHEN XU[4,6]

[1]*Sino-German College of Intelligent Manufacturing, Shenzhen Technology University, Shenzhen 518118, China*
[2]*College of Business, Shaoxing University, Shaoxing 312000, Zhejiang, China*
[3]*School of Mechanical & Electrical Engineering, PuTian University, PuTian 351100, China*
[4]*State Key Laboratory of Fluid Power and Mechatronic Systems, School of Mechanical Engineering, Zhejiang University, Hangzhou 310027, China*
[5]*pangjihong@163.com*
[6]*xukc@zju.edu.cn*

Abstract: Ultratrace molecular detections are vital for precancer diagnosis, forensic analysis, and food safety. Superhydrophobic (SH) surface-enhanced Raman scattering (SERS) sensors are regarded as an ideal approach to improve detection performance by concentrating analyte molecules within a small volume. However, due to the low adhesion of SH surfaces, the analyte droplet is prone to rolling, making it hard to deposit molecules on a predetermined position. Furthermore, the sediment with a very small area on the SH-SERS surface is difficult to be captured even with a Raman microscope. In this study, femtosecond laser fabricated hybrid SH/hydrophobic (SH/HB) surfaces are successfully applied to realize a rapid and highly sensitive SERS detection. By modulating dual surface structures and wetting behaviors, the analyte molecules can be enriched at the edge of HB pattern. This improves the convenience and speed of Raman test. On a hybrid SH/HB SERS substrate with a circular HB pattern at 300-μm-diameter, a femtomolar level (10^{-14} M) of rhodamine 6G can be detected by using analyte volumes of just 5 μL. The SERS enhancement factor can reach 5.7×10^{8} and a good uniformity with a relative standard deviation of 6.98% is achieved. Our results indicate that the laser fabrication of hybrid SERS sensor offers an efficient and cost-effective approach for ultratrace molecular detection.

1. Introduction

In recent years, food, environment, and health have become the focus of social concern. Studies find that some toxic substances with only a small dose can cause damage to the human body, so how to quickly and accurately detect the ultratrace hazardous molecular is crucial. Since its discovery in 1977, surface-enhanced Raman scattering (SERS) has been dramatically developed due to its distinct capability to trace low-concentration molecules [1–3]. It plays an important role in a variety of applications such as water pollution detection [4], explosive sensing [5], and food security monitoring [6]. The SERS enhancement is mainly attributed to chemical and electromagnetic enhancement, and the latter mechanism induced by the localized surface plasmon resonance (LSPR) is universally accepted [7–10]. In general, to prepare a test specimen for SERS detection, the SERS active rough substrate should be immersed in a solution of interest, resulting in that only a fraction of the test molecules contribute to the hot spots, yet most of the test samples are wasted [11,12]. Besides, for the applications in precancer diagnosis, forensic analysis, and food safety, the detection of ultratrace molecules is expected to be realized from the solution of small volumes. In these cases, the targeted molecules are usually randomly dispersed

#423789 https://doi.org/10.1364/OE.423789
Journal © 2021 Received 1 Mar 2021; revised 10 May 2021; accepted 10 May 2021; published 17 May 2021

Optics EXPRESS

in the highly diluted solution with a concentration as low as 10^{-15}~10^{-12} M. However, coffee ring effect on the hydrophilic SERS surface tends to hinder the targeted molecules from being concentrated to a limited area [13].

Recently, SERS substrates with superhydrophobicity were developed to resolve these problems [14,15]. When the droplets containing analytes evaporate on a low-adhesive (LA) superhydrophobic (SH) surfaces with a water contact angle (CA) over 150° and sliding angle (SA) smaller than 10°, the coffee ring effect can be effectively suppressed, which results in the enrichment of analyte molecules [13]. For example, Min et al. demonstrated a SH SERS substrate using Sn-doped indium oxide as a template, and the lowest detection concentration of rhodamine 6G (R6G) was about 10^{-8} M [16]. George et al. prepared a flexible SH surface by replicating laser-written patterns created on polymethylmethacrylate on a soft-elastomer, and a limit of detection as low as 8×10^{-15} M for R6G molecules was achieved [17]. Cao et al. prepared an SH Ag nanoparticles decorated $Cu(OH)_2$ nanoneedle array and used R6G as the probe molecule, which resulted in a detection limit approaching to approximately 0.1 ppm [18]. Moreover, the sensor could be reused by at least six cycles without any cleaning process. Notably, Tan et al. used capillary force lithography (CFL) and Langmuir–Schaefer techniques to fabricate a stable SH-SERS platform, achieving a detection limit of 10^{-17} M with 4 μL R6G [19].

Nevertheless, due to the extremely small SA, the droplet is prone to rolling on the LA-SH surface, leading to the difficulty in controlling the molecules' deposited position. Besides, for the colorless analyte with an extremely low-concentration, the sediment with a very small area on the SH-SERS substrate is hard to be captured even by a Raman microscope. Furthermore, according to Industry 4.0, production automation is required, and a high expectation is put forward for the automation of measuring instruments and test processes. At present, to realize automated sample injection and testing of SERS detection, in addition to using the automated devices, precise positioning and rapid analysis of deposited analyte molecules are essential. Therefore, concentrating the specimen to a predetermined position without losing the targeted molecules and capturing the enrichment zone rapidly with a highly sensitive detection are of great significance.

In general, SH surfaces on metal materials are usually achieved by fabricating micro-nano structures with a subsequent chemical modification procedure [20]. To fabricate hierarchical micro/nano-structures, laser texturing is a facile and efficient approach, which has been successfully applied in various fields [21,22]. In this study, femtosecond laser fabrication of hybrid SH/hydrophobic (HB) surfaces with designed patterns on stainless steels were used to realize a rapid and highly sensitive SERS detection. The patterned hierarchical micro/nano-structures can be prepared in one step. By tuning laser processing parameters, micro/nano-structures can be well regulated to determine the wetting behaviors. Relying on the differences in the structure and droplet adhesion between the HB pattern and the surrounding SH surface, the analyte molecules can be fully enriched to a predetermined position. The deposited molecules with a small area can be easily captured to complete the SERS detection rapidly. The evaporation processes of droplets on the surfaces with different wetting behaviors were investigated. Finally, the Raman spectra of analyte droplets with various concentrations were measured to confirm the feasibility of proposed techniques.

2. Experimental methods

A 50×50 mm^2 AISI304 stainless steel sheet with a thickness of 1 mm was selected as the sample substrate. The as-received substrates were cleaned in an ultrasonic ethanol bath for 10 minutes and then the surface was textured by a laser galvo-scanning system. As shown in Supplement 1, Fig. S1, a Gaussian laser beam, emitted from a 520 nm femtosecond laser (Spectra-Physics Spirit HE 1040-30-SHG) with a pulse width of 300 fs at 250 kHz pulse repetition frequency, was focused onto the sample surface by an F-Theta lens with a focal spot size of 16 μm in diameter. The sample surfaces were textured with the optimized laser processing parameters: laser fluence

Optics EXPRESS

of 2.6 J/cm^2 and scanning spacing of 50 μm. To reduce the surface energy, the laser-textured samples were then modified with a 0.01 mol/L solution of stearic acid (Sigma-Aldrich) at an ambient temperature for 60 min and dried in atmospheric conditions. Then, a layer of 60 nm thick gold film was deposited on the laser-ablated stainless steel by a high-vacuum evaporation technique (Wuhan Wakesc Technology Co., Ltd, QM-1A).

The CA, SA, and contact line (CL) were measured with 3 μL distilled water by a video optic contact angle instrument (DATAPHYSICS, OCA 25). The surface morphology of the laser textured stainless steel was characterized using a 3D measuring laser microscope (Olympus, OSL 4100) and a field-emission scanning electron microscopy SEM (Hitachi, Su 8010). A 5 μL R6G solution droplet was deposited and evaporated on the hybrid SERS substrate in the air at room temperature to conduct the Ramen detection. The Raman spectra were carried out by a Raman microscope (London, Renishaw inVia). The excitation source was a 633 nm laser with a power of 0.5 mW (50 mW in total). The laser spot size at the focus was around 1 μm in diameter with a 50× objective lens and the integration time was 3s. All the SERS spectra presented in this work were obtained by a single measurement method.

3. Results and discussion

For metal materials, SH surfaces are usually obtained via creating rough structures followed by depositing low surface energy chemical molecules [20]. Moreover, the surface morphologies can be regulated to determine the wetting modes of various artificial bionic surfaces [23]. For example, a small sliding angle below 10° is achieved by mimicking lotus leaves [24], and water drops on high-adhesion (HA) SH surfaces derived from rose petals cannot slide at any tilted angles [25]. Figures 1–2 show the wetting behaviors and surface morphologies of the laser textured stainless steel with different scanning speeds. In this experiment, laser processing is conducted by scanning the focusing spot in two perpendicular directions. For the Gaussian beam, since the average laser fluence used is much higher than the damage threshold, the surface structure can be regulated by controlling the laser spot's overlap rate [26]. When the scanning speed is 20 mm/s, the laser-ablated surface is featured with a micro/nano-scale hierarchical structure (Fig. 2(a) and Supplement 1, Fig. S2). The microscale groove (Supplement 1, Fig. S2) with a depth of 18.2 μm is caused by the removal of material. The nanoparticles (Figs. 2(c) and 2(e)) with a 20-100 nm size are induced by the rapid cooling of the ejected liquid melt in the localized melt region [27]. The air layer trapped in this type of composite structure prevents the surface from being wetted and results in a small solid/liquid contact area with a low-adhesion (LA). Therefore, after chemical modification, the laser textured surface with a low surface energy

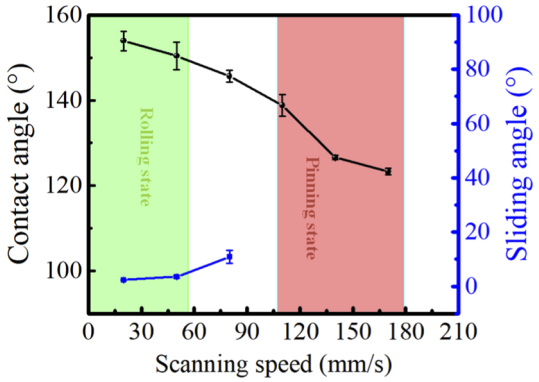

Fig. 1. Effect of laser scanning speed on CA and SA.

Optics EXPRESS

shows an excellent superhydrophobicity with an apparent CA of 153.9°, and a SA of only 2.3° (Fig. 1). However, as the overlap rate of laser spot decreases with increasing the scanning speed, the roughness of laser textured surface gradually decreases Supplement 1, Figs. S2(e) and (f)), which results in the decrease of CA and the increase of SA. Importantly, increasing the scanning speed up to 110 mm/s enables the water droplet to be firmly pinned on the SH surface without any movement at any tilted angles (Fig. 1).

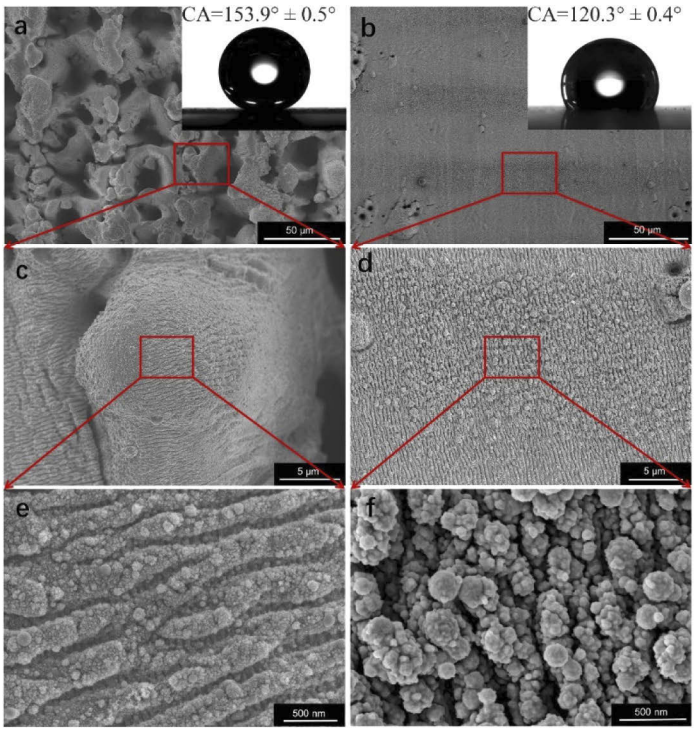

Fig. 2. SEM images of the laser-ablated surfaces at the scanning speeds of (a, c, and e) 20 mm/s, and (b, d, and f) 170 mm/s.

As illustrated in Figs. 2(b), 2(d), and 2(f), when the laser scanning speed increases to 170 mm/s, high-density nanostructures can be still observed on the material surface. Nevertheless, compared to the textured surface prepared at a speed of 20 mm/s (Fig. 2(a)), the surface shown in Fig. 2(b) is relatively flat. This higher scanning speed results in a micro-groove depth of only 2.4 μm (Supplement 1, Fig. S2), which causes the micro-scale structures to be less obvious. Moreover, the nanoparticles with a size of 80-200 nm (Fig. 2(f)) are significantly larger than those shown in Fig. 2(e). The above factors lead to complete contact and HA on solid/liquid interfaces. Hence, to maximize the differences in droplet adhesion and surface structure, the laser speeds of 20 mm/s and 170 mm/s were chosen to fabricate the LA-SH and the HA-HB surfaces, respectively.

For the SERS detection that only uses a small volume of droplet, the sediment's area after the droplet evaporating is crucial to perform the measurement. The evaporation processes of particle-laden water droplets on the solid surfaces with different wetting properties are shown in Fig. 3. For the HA-HB surface (Fig. 3(a)), the initial CA is only 120.3°. Due to the HA, the CA decreases obviously with time, and the contact line (CL) is almost pinned on the surface with only a slight decrease of ~0.03 mm. As the evaporation rate at the CL is relatively fast, a capillary flow moving from the center to the edge continuously carries the dispersed nanoparticles to the drop periphery. Finally, the analytes are deposited along the CL to form a coffee ring with a diameter

Optics EXPRESS

of 1.8 mm. On the LA-SH surface (Fig. 3(b)), the initial droplet with an extensive CA possesses a small CL. During the first 48 minutes of the evaporation process, the CA is always larger than 136°, and the CL is free to recede. Notably, the drying process can be greatly accelerated by placing the SERS substrate on a hotplate. Subsequently, the CA shows a considerable decrease, and the final contact diameter is only 0.34 mm, corresponding to an area of ~0.09 mm^2, which is 28.3 times smaller than that of the HAHS. This reveals that the LA-SH surface is beneficial to improve the SERS detection range. Nevertheless, since the droplet is easy to slide on the LA-SH surface, it is difficult to control the molecules' deposition position. Besides, for trace amount of colorless analyte on the LA-SH with a single periodic structure, the deposited particles cannot be quickly captured even using a microscopic Raman equipment.

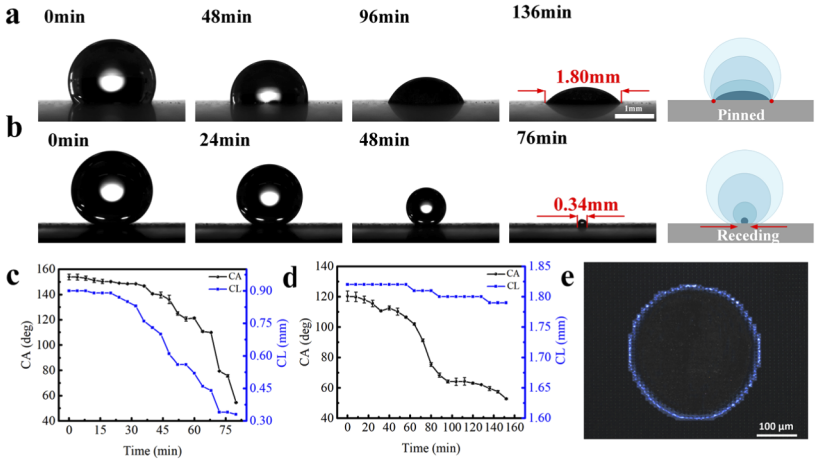

Fig. 3. Evaporation process of 5 μL drops containing 0.1 mg/mL polystyrene on (a) HA-HB and (b) LA-SH surfaces. The CA and CL as a function of evaporation time for (c) LA-SH and (d) HA-HB surfaces. (e) Optical image of polystyrene deposited on a hybrid SH/HB surface.

To concentrate molecules on the desired position, an HA-HB pattern with a diameter of 300 μm was fabricated on a LA-SH surface. When the droplet is released to the boundary between the HA-HB pattern and the surrounding LA-SH surface, it tends to be attracted by the HA pattern and pinned on the surface. During the evaporation process, the CL is on the LA-SH surface first, and then the CL shrinks to the edge of the HA pattern. Due to the coffee ring effect on the HA surface, the analyte is deposited along the edge (Fig. 3(e)). Besides, as shown in Fig. 4, the 3D profile shows that the surface roughness of the HA hydrophobic pattern and the surrounding LA-SH is 1.71 μm and 5.28 μm, respectively. Based on the different surface structures, the analyte deposited along the HA pattern's edge is easy to be captured using a Raman microscope. Meanwhile, the surface nanostructure is beneficial to enhancing the Raman signal (Figs. 2(e)–2(f)), verified by previous research [28,29]. The so-called "hot spots" are formed among adjacent nanoparticles, which can significantly enhance the electric field and improve the SERS density [30–32].

The HA hydrophobic patterns with different sizes (Figs. 5(a)–5(c)) can lead to various SERS performances. After 60 nm gold film was deposited on the laser-ablated stainless steel, R6G was chosen as a probe molecule to investigate the SERS activity of the patterned SH/HB surface. For comparison, three circular HA-HB patterns with diameters of 400 μm, 300 μm, and 200 μm were made on the LA-SH surface. As shown in Fig. 5(d), after a 5 μL R6 G droplet with a concentration of 10^{-6} M deposited on the patterned surface, characteristic Raman peaks are able to be observed at 611, 775, 1188, 1313, and 1362 cm^{-1}, respectively. The most substantial peaks occur at 611 cm^{-1}, which is selected for the comparison experiment. When the diameter

Optics EXPRESS

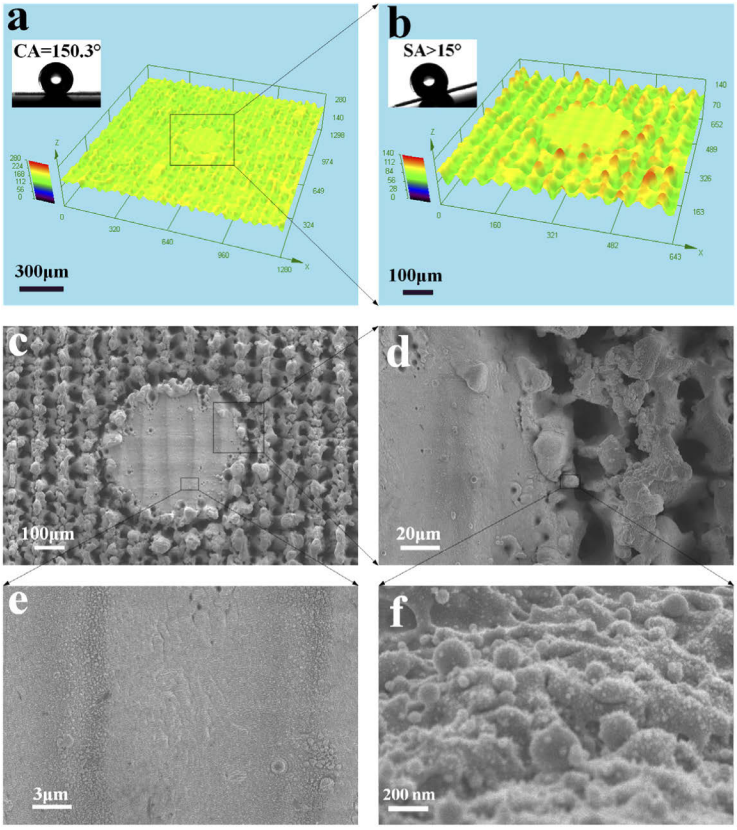

Fig. 4. Images of the femtosecond laser patterned surface. (a), (b) 3D profile of the surface. (c)-(f) SEM images of the hybrid SH/HB surfaces.

of HA-HB pattern is 400 μm, a SERS intensity of 6110 counts is obtained. As the diameter decreases to 300 μm, the Raman signal shows the maximum intensity of 8492 counts. This is because the reduction in the HA-HB pattern size is beneficial to enriching the target molecules. However, further decreasing the HA-HB pattern reduces the SERS intensity to 4830 counts. This is due to that the sediment's area cannot be infinitely reduced with the shrinkage of HA-HB (Supplement 1, Fig. S3). During the analyte droplet's evaporation process on the HA-HB pattern with a diameter of 200 μm, partial targeted molecules are deposited on the surrounding LA-SH surface, resulting in the decrease of Raman signals (Supplement 1, Fig. S3). This matches well with the findings by Chen et al. [33].

Figure 5(e) shows the Raman signals at different regions marked in Fig. 5(b). It can be seen that the Raman signal in region 2 is significantly stronger than that in region 1 and 3. The major reason is that the target molecules are mainly concentrated along the HA-HB pattern' edge, corresponding to region 2. This can also be confirmed by the micrographs of analytes distributed on hybrid SH/HB surfaces as shown in Supplement 1, Fig. S3. Therefore, the subsequent Raman signals were all measured at the edges of HA-HB patterns.

For SERS applications, detection limit is a significant indicator. Figure 6(a) shows the Raman signals of 10^{-6}, 10^{-8}, 10^{-10}, 10^{-12}, 10^{-13}, and 10^{-14} M R6 G on the patterned SH/HB surfaces. By analyzing the peak at 611 cm^{-1}, a quantitative comparison of the SERS intensities across various R6 G concentrations, ranging from 10^{-10} M to 10^{-6} M, demonstrates that a linear SERS response is obtained (Fig. 6(b)). The error bars refer to 3 measurements on a single SERS

Optics EXPRESS

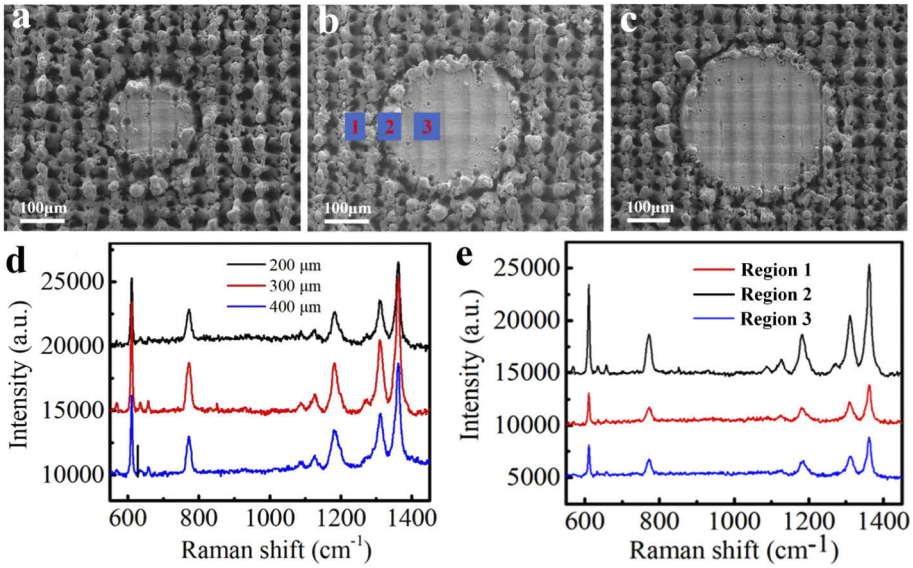

Fig. 5. SEM images of the hybrid SH/HB surfaces, on which the diameters of the HB patterns are (a) 200 μm, (b) 300 μm, and (c) 400 μm, respectively. (d) Raman spectra of 10^{-6} M R6G solutions at the edges of different HB patterns. (e) Raman spectra of 10^{-6} M R6G solutions at region 1, 2, and 3.

substrate with a 300 μm diameter circular HB pattern, and the test was carried out by randomly selecting 3 points at the edge of HA-HB pattern. The distinct peaks of R6 G can be seen even down to a concentration of 10^{-14} M. This indicates the proposed SERS sensors are able to trace extremely low-concentration analytes.

The analytical enhancement factor is calculated to quantify the improvement of SERS enhancement of analyte molecules concentrated on the patterned SH/HB substrate. Based on the reported method [19], the corresponding enhancement factor (EF) can be calculated by the following equation:

$$\mathrm{EF} = \frac{I_{SERS} \times \mathrm{C_{Raman}}}{I_{\mathrm{Raman}} \times \mathrm{C}_{SERS}}. \tag{1}$$

where I_{SERS} and I_{Raman} stand for the signal intensities collected from SERS and normal Raman substrate, respectively. C_{SERS} and C_{Raman} are the corresponding detection limit concentrations achieved on the hybrid SH/HB platform and hydrophilic normal Raman platform, respectively. Based on the signal at 611 cm^{-1}, an EF on the order of ~5.7×10^{8} is obtained for the as-prepared hybrid SH/HB SERS sensor.

High SERS signal homogeneity and repeatability of the patterned SH/HB SERS substrate is further demonstrated by the SERS imaging (Fig. 6(c)). Using the SERS spectra at 10^{-6} M R6G as an example, we randomly selected 8 points on the patterned SH/HB substrate to measure the Raman signal. The results show that the SERS substrate demonstrates a uniform SERS signal distribution across the region where R6G is deposited after drying. The relative standard deviation (RSD) of the Raman intensity at 611 cm^{-1} is as low as 6.98% (Fig. 6(d)). Furthermore, additional seven hybrid SERS substrates with circular HB patterns at 300-μm-diameter were fabricated (Supplement 1, Fig. S4). The RSD of Raman intensity for the different SERS substrates is 8.11%, indicating a relatively high reproducibility.

Optics EXPRESS

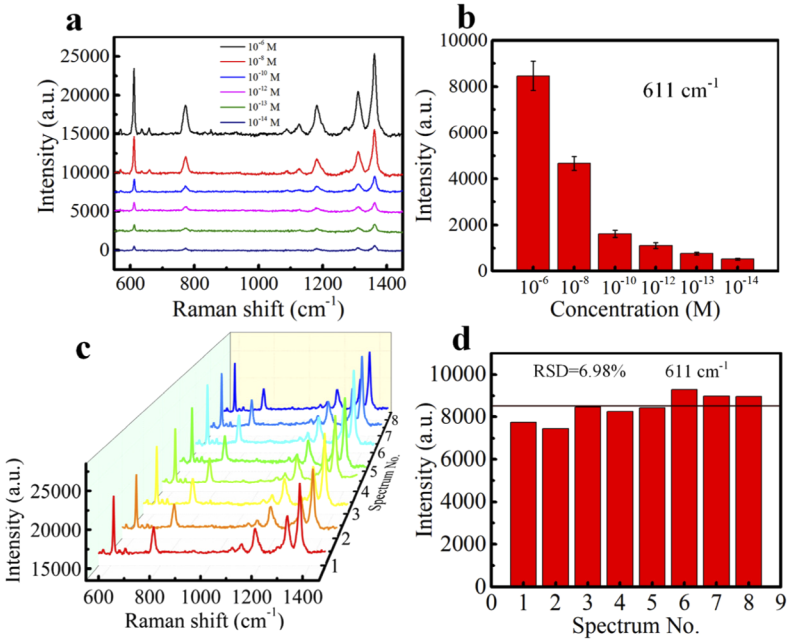

Fig. 6. (a) Raman spectra of R6G at different concentrations. (b) SERS intensities at 611 cm^{-1} for R6G concentrations ranging from 10^{-14} to 10^{-6} M. (c) Raman signals of eight random points at the edge of HB pattern adsorbed with 10^{-6} M R6G analytes. (d) Comparison of SERS intensities using the eight SERS spectra extracted from (c).

4. Conclusion

In summary, rapid and highly sensitive SERS detection has been successfully achieved on hybrid SH/HB surfaces fabricated by a selective laser texturing method. Femtosecond laser is a facile and efficient tool to regulate the surface structures and wetting behaviors. Based on the difference in the surface structures and wetting behaviors of the SH and HB surfaces, the analyte droplet can be accurately concentrated to the HB pattern's edge. Therefore, the detection limit is significantly improved, and the Raman test becomes easy and rapid. On a hybrid SH/HB SERS substrate with a 300 μm diameter circular HB pattern, a highly diluted solution (R6G) with concentrations as low as 10^{-14} M can be detected by using only 5 μL volume. The SERS EF can reach 5.7×10^{8}, which is sufficient for molecular-level detection. The research results suggest that this simple, cost-effective SERS sensor's fabrication method could open up opportunities in ultratrace detection applications, such as precancer diagnosis, forensic analysis, and food safety monitoring.

Funding. Key Laboratory of Functional Materials and Applications of Fujian Province (2018XKA001); Colleges Innovation Project of Guangdong (2018KTSCX347, 2020KQNCX070); National Natural Science Foundation of China (71671130, 72071149); Natural Science Foundation of Top Talent of SZTU (2020103).

Disclosures. The authors declare that there are no conflicts of interest related to this article.

Data availability. Data underlying the results presented in this paper are not publicly available at this time but may be obtained from the authors upon reasonable request.

Supplemental document. See Supplement 1 for supporting content.

Optics EXPRESS

References

1. F. Chu, S. Yan, J. Zheng, L. Zhang, H. Zhang, K. Yu, X. Sun, A. Liu, and Y. Huang, "A simple laser ablation-assisted method for fabrication of superhydrophobic SERS substrate on teflon film," Nanoscale Res. Lett. **13**(1), 244–252 (2018).
2. X. Zhao, J. Yu, C. Zhang, C. Chen, S. Xu, C. Li, Z. Li, S. Zhang, A. Liu, and B. Man, "Flexible and stretchable SERS substrate based on a pyramidal PMMA structure hybridized with graphene oxide assivated AgNPs," Appl. Surf. Sci. **455**, 1171–1178 (2018).
3. K. Xu, Z. Wang, C. F. Tan, N. Kang, L. Chen, L. Ren, E. S. Thian, G. W. Ho, R. Ji, and M. Hong, "Uniaxially stretched flexible surface plasmon resonance film for versatile surface enhanced Raman scattering diagnostics," ACS Appl. Mater. Interfaces **9**(31), 26341–26349 (2017).
4. V. Iancu, L. Baia, N. Tarcea, J. Popp, and M. Baia, "Towards TiO2-Ag porous nanocomposites based SERS sensors for chemical pollutant detection," J. Mol. Struct. **1073**, 51–57 (2014).
5. M. S. Satya Bharati, B. Chandu, and S. V. Rao, "Explosives sensing using Ag–Cu alloy nanoparticles synthesized by femtosecond laser ablation and irradiation," RSC Adv. **9**(3), 1517–1525 (2019).
6. C. Leiterer, D. Zopf, B. Seise, F. Jahn, K. Weber, J. Popp, D. Cialla-May, and W. Fritzsche, "Fast self-assembly of silver nanoparticle monolayer in hydrophobic environment and its application as SERS substrate," J. Nanopart. Res. **16**(9), 2467–2474 (2014).
7. Z. Yin, K. Xu, S. Jiang, D. Luo, R. Chen, C. Xu, P. Shum, and Y. J. Liu, "Recent progress on two-dimensional layered materials for surface enhanced Raman spectroscopy and their applications," Mater. Today Phys. **18**, 100378 (2021).
8. C. Zhu, X. Hu, and X. Wang, "Silver nanocubes/graphene oxide hybrid film on a hydrophobic surface for effective molecule concentration and sensitive SERS detection," Appl. Surf. Sci. **470**, 423–429 (2019).
9. S. Y. Ding, E. M. You, Z. Q. Tian, and M. Moskovits, "Electromagnetic theories of surface-enhanced Raman spectroscopy," Chem. Soc. Rev. **46**(13), 4042–4076 (2017).
10. K. Xu, R. Zhou, K. Takei, and M. Hong, "Toward flexible surface-enhanced Raman scattering (SERS) sensors for point-of-care diagnostics," Adv. Sci. **6**(16), 1900925 (2019).
11. L. Jiang, D. Ying, X. Li, and Y. Lu, "Two-step femtosecond laser pulse train fabrication of nanostructured substrates for highly surface-enhanced Raman scattering," Opt. Lett. **37**(17), 3648–3650 (2012).
12. K. Xu, H. Yan, C. F. Tan, Y. Lu, Y. Li, G. W. Ho, R. Ji, and M. Hong, "Hedgehog inspired CuO nanowires/Cu2O composites for broadband visible-light-driven recyclable surface enhanced Raman scattering," Adv. Opt. Mater. **6**(7), 1701167 (2018).
13. A. Wang, L. Jiang, X. Li, Q. Xie, B. Li, Z. Wang, K. Du, and Y. Lu, "Low-adhesive superhydrophobic surface-enhanced Raman spectroscopy substrate fabricated by femtosecond laser ablation for ultratrace molecular detection," J. Mater. Chem. B **5**(4), 777–784 (2017).
14. Z.-X. Yan, Y.-L. Zhang, W. Wang, X.-Y. Fu, H.-B. Jiang, Y.-Q. Liu, P. Verma, S. Kawata, and H.-B. Sun, "Superhydrophobic SERS Substrates based on silver-coated reduced Graphene oxide gratings prepared by two-beam laser interference," ACS Appl. Mater. Interfaces **7**(49), 27059–27065 (2015).
15. X. Luo, R. Pan, M. Cai, W. Liu, C. Chen, G. Jiang, X. Hu, H. Zhang, and M. Zhong, "Atto-Molar Raman detection on patterned superhydrophilic-superhydrophobic platform via localizable evaporation enrichment," Sens. Actuators, B **326**, 128826 (2021).
16. K. Min, K. S. Choi, W. J. Jeon, D. K. Lee, S. Oh, J. Lee, J.-Y. Choi, and H. K. Yu, "Hierarchical Ag nanostructures on Sn-doped indium oxide nano-branches: super-hydrophobic surface for surface-enhanced Raman scattering," RSC Adv. **8**(23), 12927–12932 (2018).
17. J. E. George, V. K. Unnikrishnan, D. Mathur, S. Chidangil, and S. D. George, "Flexible superhydrophobic SERS substrates fabricated by in situ reduction of Ag on femtosecond laser-written hierarchical surfaces," Sens. Actuators, B **272**, 485–493 (2018).
18. Y. Gao, N. Yang, T. You, C. Zhang, and P. Yin, "Superhydrophobic "wash free" 3D nanoneedle array for rapid, recyclable and sensitive SERS sensing in real environment," Sens. Actuators, B **267**, 129–135 (2018).
19. J. M. Rui Tan, J. J. Ruan, H. K. Lee, I. Y. Phang, and X. Y. Ling, "A large-scale superhydrophobic surface-enhanced Raman scattering (SERS) platform fabricated via capillary force lithography and assembly of Ag nanocubes for ultratrace molecular sensing," Phys. Chem. Chem. Phys. **16**(48), 26983–26990 (2014).
20. J. Yong, J. Huo, Q. Yang, F. Chen, Y. Fang, X. Wu, L. Liu, X. Lu, J. Zhang, and X. Hou, "Femtosecond laser direct writing of porous network microstructures for fabricating super-slippery surfaces with excellent liquid repellence and anti-cell proliferation," Adv. Mater. Interfaces **5**(7), 1701479 (2018).
21. K. Sun, H. Yang, W. Xue, A. He, D. Zhu, W. Liu, K. Adeyemi, and Y. Cao, "Anti-biofouling superhydrophobic surface fabricated by picosecond laser texturing of stainless steel," Appl. Surf. Sci. **436**, 263–267 (2018).
22. K. Xu, C. Zhang, R. Zhou, R. Ji, and M. Hong, "Hybrid micro/nano-structure formation by angular laser texturing of Si surface for surface enhanced Raman scattering," Opt. Express **24**(10), 10352–10358 (2016).
23. J.-N. Wang, Y.-Q. Liu, Y.-L. Zhang, J. Feng, and H.-B. Sun, "Pneumatic smart surfaces with rapidly switchable dominant and latent superhydrophobicity," NPG Asia Mater. **10**(2), e470 (2018).
24. H. Yang, K. Xu, C. Xu, D. Fan, Y. Cao, W. Xue, and J. Pang, "Femtosecond laser fabricated elastomeric superhydrophobic surface with stretching-enhanced water repellency," Nanoscale Res. Lett. **14**(1), 333 (2019).

Optics EXPRESS

25. X. Yang, X. Liu, Y. Lu, J. Song, S. Huang, S. Zhou, Z. Jin, and W. Xu, "Controllable water adhesion and anisotropic sliding on patterned superhydrophobic surface for droplet manipulation," J. Phys. Chem. C **120**(13), 7233–7240 (2016).
26. H. Yang, D. Fu, M. Jiang, J. Duan, F. Zhang, X. Zeng, and U. Bach, "Ultraviolet laser ablation of fluorine-doped tin oxide thin films for dye-sensitized back-contact solar cells," Thin Solid Films **531**, 519–524 (2013).
27. D. Serien and K. Sugioka, "Fabrication of three-dimensional proteinaceous micro- and nano-structures by femtosecond laser cross-linking," Opto-Electron. Adv. **1**(3), 180008 (2018).
28. T. Zhang, Y. Sun, L. Hang, H. Li, G. Liu, X. Zhang, X. Lyu, W. Cai, and Y. Li, "Periodic porous alloyed Au-Ag nanosphere arrays and their highly sensitive SERS performance with good reproducibility and high density of hotspots," ACS Appl. Mater. Interfaces **10**(11), 9792–9801 (2018).
29. C. Kuttner, M. Mayer, M. Dulle, A. Moscoso, J. M. Lopez-Romero, S. Foerster, A. Fery, J. Perez-Juste, and R. Contreras-Caceres, "Seeded growth synthesis of gold nanotriangles: size control, SAXS analysis, and SERS performance," ACS Appl. Mater. Interfaces **10**(13), 11152–11163 (2018).
30. S. J. Lee, A. R. Morrill, and M. Moskovits, "Hot spots in silver nanowire bundles for surface-enhanced Raman spectroscopy," J. Am. Chem. Soc. **128**(7), 2200–2201 (2006).
31. P. Li, B. Ma, L. Yang, and J. Liu, "Hybrid single nanoreactor for in situ SERS monitoring of plasmon-driven and small Au nanoparticles catalyzed reactions," Chem. Commun. **51**(57), 11394–11397 (2015).
32. X. Lin, W.-L.-J. Hasi, X.-T. Lou, S. Lin, F. Yang, B.-S. Jia, Y. Cui, D.-X. Ba, D.-Y. Lin, and Z.-W. Lu, "Rapid and simple detection of sodium thiocyanate in milk using surface-enhanced Raman spectroscopy based on silver aggregates," J. Raman Spectrosc. **45**(2), 162–167 (2014).
33. Y. Chen, L.-P. Xu, J. Meng, S. Deng, L. Ma, S. Zhang, X. Zhang, and S. Wang, "Superwettable microchips with improved spot homogeneity toward sensitive biosensing," Biosens. Bioelectron. **102**, 418–424 (2018).